6062 *Biochemistry* **2009,** *48,* 6062–6071
DOI: 10.1021/bi9002277

BIOCHEMISTRY
including biophysical chemistry & molecular biology
Article

Structure and Dynamics of the Iron−Sulfur Cluster Assembly Scaffold Protein IscU and Its Interaction with the Cochaperone HscB[†,‡]

Jin Hae Kim,[§] Anna K. Füzéry,[∥] Marco Tonelli,[⊥] Dennis T. Ta,[@] William M. Westler,[⊥] Larry E. Vickery,[@] and John L. Markley*[,§,∥,⊥]

[§]*Biophysics Graduate Program,* [∥]*Department of Biochemistry, and* [⊥]*National Magnetic Resonance Facility at Madison, University of Wisconsin, Madison, Wisconsin 53706, and* [@]*Department of Physiology and Biophysics, University of California, Irvine, California 92697*

Received February 10, 2009; Revised Manuscript Received June 2, 2009

ABSTRACT: IscU is a scaffold protein that functions in iron−sulfur cluster assembly and transfer. Its critical importance has been recently underscored by the finding that a single intronic mutation in the human *iscu* gene is associated with a myopathy resulting from deficient succinate dehydrogenase and aconitase [Mochel, F., Knight, M. A., Tong, W. H., Hernandez, D., Ayyad, K., Taivassalo, T., Andersen, P. M., Singleton, A., Rouault, T. A., Fischbeck, K. H., and Haller, R. G. (2008) *Am. J. Hum. Genet. 82*, 652−660]. IscU functions through interactions with a chaperone protein HscA and a cochaperone protein HscB. To probe the molecular basis for these interactions, we have used NMR spectroscopy to investigate the solution structure of IscU from *Escherichia coli* and its interaction with HscB from the same organism. We found that wild-type apo-IscU in solution exists as two distinct conformations: one largely disordered and one largely ordered except for the metal binding residues. The two states interconvert on the millisecond time scale. The ordered conformation is stabilized by the addition of zinc or by the single-site IscU mutation, D39A. We used apo-IscU(D39A) as a surrogate for the folded state of wild-type IscU and assigned its NMR spectrum. These assignments made it possible to identify the region of IscU with the largest structural differences in the two conformational states. Subsequently, by following the NMR signals of apo-IscU(D39A) upon addition of HscB, we identified the most perturbed regions as the two N-terminal β-strands and the C-terminal α-helix. On the basis of these results and analysis of IscU sequences from multiple species, we have identified the surface region of IscU that interacts with HscB. We conclude that the IscU−HscB complex exists as two (or more) distinct states that interconvert at a rate much faster than the rate of dissociation of the complex and that HscB binds to and stabilizes the ordered state of apo-IscU.

Iron−sulfur (Fe−S) proteins play indispensable roles in electron transfer, catalysis, and gene regulation (*1*). The prosthetic group of Fe−S proteins, the Fe_nS_n cluster, comes in a variety of sizes and geometries and includes 2Fe-2S, 3Fe-4S, and 4Fe-4S clusters (*2*). The functional importance of Fe−S proteins spurred investigations of cluster assembly mechanisms and led to the discovery of the Nif (nitrogen fixation), Isc (iron−sulfur cluster), and Suf (sulfur utilization factor) assembly systems (*2*). Of these three systems, the Isc system is responsible for generalized Fe−S cluster biosynthesis in most organisms (*2*, *3*).

The Isc operon of *Escherichia coli* encodes several protein products: IscR,[1] IscS, IscU, IscA, HscB, HscA, and Fdx (*2*). Of these components, IscU is particularly important because it acts as a scaffold on which the cluster is assembled and from which the cluster is subsequently transferred to a recipient apoprotein (*4*). It has been reported that the Asp39Ala (D39A) substitution in *Azotobacter vinelandii* IscU (*5*), or in the corresponding IscU variants from *Aquifex aeolicus* (*6*), *Schizosaccharomyces pombe* (*7*), and *Homo sapiens* (*8*), stabilizes the cluster-coordinating complex of IscU. This stabilization

[†]This work was supported by National Institutes of Health (NIH) Grants R01 GM58667 (J.L.M.) and GM 54624 (L.E.V.). NMR data were collected at the National Magnetic Resonance Facility at Madison (NMRFAM) with support from NIH Grants P41 RR02301 (J.L.M.) and P41 GM66326 (J.L.M.).

[‡]^{1}H, ^{13}C, and ^{15}N resonance assignments and ^{15}N R_1, R_2, and heteronuclear NOE values of apo-IscU(D39A) were deposited in the BioMagResBank as entry 7432. ^{1}H and ^{15}N resonance assignments of IscU(D39A) in the complex with HscB were deposited as entry 15967.

*To whom correspondence should be addressed. Phone: (608) 263-9349. Fax: (608) 262-3759. E-mail: markley@nmrfam.wisc.edu.

[1]Abbreviations: DTT, dithiothreitol; DSS, 2,2-dimethyl-2-silapentane-5-sulfonic acid; HscB/A, heat shock cognate protein B/A; Hsp, heat shock protein; HSQC, heteronuclear single-quantum coherence; IPTG, isopropyl β-D-1-thiogalactopyranoside; IscR, -S, -U, and -A, iron−sulfur cluster proteins R, S, U, and A, respectively; IscU, unless noted otherwise, IscU from *Escherichia coli*; IscU(D39A), IscU mutant in which aspartate at residue 39 is replaced with alanine; ITC, isothermal titration calorimetry; NMR, nuclear magnetic resonance; NOE, nuclear Overhauser effect; PDB, Protein Data Bank; PECAN, protein energetic conformational analysis from NMR chemical shifts; SBD, substrate binding domain; TROSY, transverse relaxation-optimized spectroscopy; [U-^{15}N], uniformly ^{15}N-labeled.

Published on Web 06/03/2009

has been attributed to a decrease in the solvent accessibility of the cluster (*9*, *10*).

In vitro experiments have shown that holo-IscU is able to transfer its cluster to an apoprotein but that the presence of HscA and HscB greatly enhances the rate and efficiency of this process (*11*, *12*). HscA and HscB are specialized versions of an Hsp70-type chaperone and an Hsp40-type cochaperone, respectively. The nature of the nucleotide (ATP or ADP) bound to HscA allosterically regulates the affinity of the chaperone for IscU (*13*), and the ATPase activity of HscA is greatly enhanced by its interaction with HscB and IscU (*14*). The differential affinity of HscA for IscU and the role of HscB in enhancing the binding of IscU to HscA and increasing the ATPase activity of HscA appear to regulate the cycle of cluster transfer from IscU to a protein such as apoferredoxin (*11*, *12*).

Our understanding of Fe−S cluster transfer has also been aided by structural investigations of IscU, HscA, HscB, and complexes of these proteins. The NMR solution structures of Zn-bound IscU from *Haemophilus influenzae* (*15*) and *Mus musculus* (PDB entry 1wfz) indicated that the Zn-bound protein has a compact structural core that consists of two α-helices (α2 and α5) packed against a three-stranded antiparallel *β*-sheet (*β*1−*β*3) on one side and two short α-helices (α3 and α4) on the other. The NMR solution structure of Zn-bound *H. influenzae* IscU (*15*) shows the Zn atom coordinated by two cysteines located in the loop region (C37 and C63) and one histidine and one cysteine at the edge of helix α5 (H105 and C106). In the absence of zinc, *H. influenzae* IscU was found to be much less structured (*15*). Consistent with an inherent structural flexibility, the recently determined crystal structure of holo-IscU from *A. aeolicus* revealed a different conformation for each of the three IscU monomers within the trimeric holo complex (*16*). In addition, apo-SufU of *Thermotoga maritima* (an IscU counterpart in the Suf system) was reported to have a molten globule-like tertiary structure consisting of multiple conformations (*17*, *18*). The best model for the interaction between IscU and HscA comes from the X-ray structure of the substrate binding domain (SBD) of HscA cocrystallized with ELPPVKIHC (*19*), an IscU-derived peptide that was shown to interact with HscA (*20*, *21*). The crystal structure revealed that the ELPPVKIHC peptide binds to the hydrophobic cleft of HscA(SBD) in a fully extended conformation, implying a significant conformational change in IscU as a result of the binding interaction with HscA (*19*). The binding interaction between apo-IscU and HscB involves the formation of a 1:1 complex with a dissociation constant of ≅13 *μ*M (*14*). A recent NMR spectroscopic study proposed that the binding site for IscU is located on one face of HscB's C-terminal domain and contains several highly conserved hydrophobic as well as acidic residues (*22*). Furthermore, alanine shaving experiments suggested that the hydrophobic residues (L92, M93, and F153 in *E. coli* HscB) may play an important role in strengthening the binding interaction (*22*).

We report here the results from a complementary investigation of *E. coli* apo-IscU and its interaction with *E. coli* HscB. Our study indicates that apo-IscU exists in solution in two conformational states, one largely disordered and one ordered with the exception of the metal binding region. The ordered structure resembles that stabilized by the addition of Zn^{2+}. A single-site mutation, IscU(D39A), leads to the stabilization of the ordered state. Our results identify residues of IscU that are perturbed upon the addition of the cochaperone HscB and provide information about the nature of the IscU−HscB complex.

EXPERIMENTAL PROCEDURES

Materials. BL21 competent cells were obtained from Novagen (Madison, WI), and strain JM15 [CGSC strain 5042 (*23*)] was obtained from the *E. coli* Genetic Stock Center (EGSC) of Yale University (New Haven, CT). The QuikChange II site-directed mutagenesis kit was purchased from Stratagene (Cedar Creek, TX). $^{15}NH_4Cl$ and [U-^{13}C]-D-glucose were purchased from Cambridge Isotope Laboratories (Andover, MA). Other chemicals, including natural abundance amino acids and chemicals for buffers, were purchased from Sigma-Aldrich Corp. (St. Louis, MO). DE-52 anion exchange resin was purchased from Whatman Inc. (Florham Park, NJ). DEAE Bio-Gel anion exchange gel was purchased from Bio-Rad Laboratories (Hercules, CA), and the HiLoad 16/60 Superdex 75 prep grade gel filtration column was purchased from GE Healthcare Bio-Sciences Corp. (Piscataway, NJ).

Site-Directed Mutagenesis. To express IscU(D39A), the QuikChange technique was used to introduce the appropriate mutation into the pTrcIscU expression vector (*14*). The presence of the mutation in the new expression vector [henceforth called pTrcIscU(D39A)] was subsequently confirmed by DNA sequencing.

Expression and Purification of Proteins. HscB was expressed and purified as described previously (*14*). [U-^{15}N]- and [U-^{13}C,U-^{15}N]-labeled samples of IscU and IscU(D39A) were prepared as follows. A colony of BL21 cells transformed with the pTrcIscU [or pTrcIscU(D39A)] plasmid was used to inoculate 10 mL of TB liquid medium containing 100 *μ*g/mL ampicillin. The cells were grown for ∼12 h at 37 °C, and a 10 *μ*L inoculum was transferred to 50 mL of TB liquid medium containing 100 *μ*g/mL ampicillin, which was subsequently grown for ∼12 h at 37 °C. Cells from this 50 mL culture were used to inoculate 500 mL of M9 medium containing 100 *μ*g/mL ampicillin and supplemented with either 0.5 g of $^{15}NH_4Cl$ and 2.5 g of glucose (for production of [U-^{15}N]IscU) or 0.5 g of $^{15}NH_4Cl$ and 1.5 g of [U-^{13}C]-D-glucose (for production of [U-^{13}C,U-^{15}N]IscU). Gene expression was induced at an Abs_{600} of ≈1 by adding IPTG to a final concentration of 0.4 mM. Protein production was allowed to proceed for ∼3 h, after which cells were harvested and stored at −80 °C. Protein purification was conducted as described previously (*14*), except that a HiLoad 16/60 Superdex 75 gel filtration column was employed for the final purification step in place of reversed phase chromatography. The elution buffer for this step consisted of 20 mM Tris-HCl (pH 8.0), 1 mM DTT, 0.5 mM EDTA, and 150 mM NaCl.

IscU(D39A) was further characterized to determine whether it serves as a suitable model for investigating the interaction between wild-type IscU and HscB. The affinity of apo-IscU (D39A) for HscB was determined directly using isothermal titration calorimetry. Figure S1 (Supporting Information) shows that apo-IscU(D39A) forms a 1:1 complex with HscB with a binding affinity of ≅10 *μ*M and thermodynamic parameters similar to those observed with apo-IscU (*14*, *21*). We also measured the ability of apo-IscU(D39A) to stimulate the ATPase activity of HscA, a sensitive probe for monitoring the binding interactions among HscA, IscU, and HscB (*14*, *21*). As shown in Figure S2 (Supporting Information), apo-IscU(D39A) acts synergistically with HscB to stimulate HscA ATPase activity in a manner similar to that observed for wild-type IscU (*14*), indicating that apo-IscU(D39A) interacts with HscB and HscA in a physiologically relevant manner.

Selective Isotopic Labeling. To produce proteins selectively reverse-labeled with an amino acid of natural abundance, 500 mL of M9 growth medium containing 100 μg/mL ampicillin was initially supplemented with 0.5 g of $^{15}NH_4Cl$ and 1 g of glucose. When the cell culture reached an Abs_{600} of $\approx$1, the following additions were made: IPTG (final concentration of 0.4 mM), 1 g of glucose, and an unlabeled amino acid (0.28 g of glycine to produce [U-^{15}N,^{14}N-Gly]IscU, 0.2 g of L-arginine-HCl to produce [U-^{15}N,^{14}N-Arg]IscU, or 0.2 g of L-lysine-HCl to produce [U-^{15}N,^{14}N-Lys]IscU) (*24*). To prepare [U-^{15}N,^{14}N-Cys]IscU, a Cys-auxotrophic strain of JM15 cells (*23*) was transformed with the pTrcIscU(D39A) plasmid. Initial cell growth was conducted as described above for BL21 cells, but later steps were modified as follows. Cells from the 50 mL of TB medium were used to inoculate 125 mL of TB medium, which was subsequently grown overnight at 37 °C. Cells from the 125 mL of TB medium were transferred to 500 mL of M9 medium supplemented with 0.5 g of $^{15}NH_4Cl$ and 1 g of glucose. Following incubation for ~2 h, the following was added: IPTG (to a final concentration of 0.4 mM), 1 g glucose, and 0.03 g of L-cysteine. After further incubation for ~3 h, the cells were harvested and stored, and proteins were purified as described above.

NMR Samples. The solvent used for NMR samples contained 20 mM Tris-HCl (pH 8.0), 0.5 mM EDTA, 5−10 mM DTT, 150 mM NaCl, 7% D_2O, 0.7 mM DSS, and 0.02% sodium azide. A sample of 0.8 mM [U-^{15}N]apo-IscU was employed to obtain two-dimensional (2D) NMR spectra, while a sample of 2.0 mM [U-^{13}C,U-^{15}N]apo-IscU was used to collect three-dimensional (3D) NMR spectra. To prepare Zn^{2+}-bound IscU, 0.8 mM [U-^{15}N]IscU was exchanged into 20 mM Tris-HCl (pH 8.0), 3 mM $ZnCl_2$, 5−10 mM DTT, 150 mM NaCl, 7% D_2O, 0.7 mM DSS, and 0.02% sodium azide. The concentration of [U-^{13}C,U-^{15}N]apo-IscU(D39A) used for resonance assignments was 2.5 mM. The concentration of [U-^{15}N]apo-IscU (D39A) used for ^{15}N relaxation and ^{1}H−^{15}N heteronuclear NOE measurements was 0.6−0.7 mM. Chemical shift perturbation experiments started with a sample of 0.6−0.8 mM [U-^{15}N]IscU(D39A) to which were added aliquots of 2.5 mM unlabeled HscB.

NMR Spectroscopy. Unless specified otherwise, all NMR spectra were acquired at 25 °C with 600 or 800 MHz Varian Unity-Inova spectrometers equipped with a *z*-gradient cold probe. NMRPipe (*25*) was used to process the raw NMR data, and Sparky (*26*) was used for data analysis. The 2D exchange experiment (*27*, *28*) with apo-IscU was conducted on a 750 MHz Bruker DMX spectrometer equipped with a CryoProbe. The mixing time used to detect chemical exchange was set to 60 ms. The following data sets were collected and used to assign the resonances from [U-^{13}C,U-^{15}N]IscU(D39A): 2D ^{15}N HSQC, 3D HNCO, 3D CBCA(CO)NH, 3D HNCACB, 3D HN(CO)CA, 3D HNCA, and 2D ^{15}N NOESY-HSQC (τ_m = 100 ms). 2D ^{15}N HSQC spectra of selectively reverse-labeled IscU(D39A) [[U-^{15}N,^{14}N-Arg]IscU(D39A), [U-^{15}N,^{14}N-Gly]-IscU(D39A), [U-^{15}N,^{14}N-Lys]IscU(D39A), and [U-^{15}N,^{14}N-Cys]IscU(D39A)] were also used to assign ambiguous resonances. Chemical shift assignments were used as input for the PECAN web server (*29*) to predict the secondary structure of IscU(D39A). We made resonance assignments of apo-IscU with the help of the apo-IscU(D39A) assignments and by collecting and analyzing 2D ^{15}N HSQC, 3D HNCO, 3D CBCA(CO)NH, 3D HNCACB, and 3D HNCA spectra. The tendency of a certain residue to form a secondary structural element in apo-IscU was predicted by comparing the difference between the secondary $^{13}C^{\alpha}$ and $^{13}C^{\beta}$ chemical shifts of apo-IscU with the difference between $^{13}C^{\alpha}$ and $^{13}C^{\beta}$ chemical shifts of a random coil (for Gly residues, only $^{13}C^{\alpha}$ chemical shifts were compared) (*30*, *31*).

R_1 and R_2 relaxation and ^{1}H−^{15}N heteronuclear NOE data sets of [U-^{15}N]apo-IscU(D39A) were acquired at 25 °C on a 600 MHz Varian Unity-Inova spectrometer equipped with a *z*-gradient cold probe. R_1 relaxation rate experiments utilized relaxation delays of 100, 200, 300, 400, 600, 800, and 1200 ms; R_2 relaxation rate experiments utilized relaxation delays of 10, 30, 50, 70, 90, 110, and 130 ms. The ^{1}H excitation time in the ^{1}H−^{15}N heteronuclear NOE experiments was set to 3 s, and the intensities of each peak in spectra collected with and without the ^{1}H excitation were compared to determine the NOE value. Two replicate sets of R_1, R_2, and ^{1}H−^{15}N NOE data were collected; standard deviations were estimated from their differences, and the replicate values were averaged to yield the reported values.

For chemical shift perturbation measurements, HscB was titrated into a solution of [U-^{15}N]IscU(D39A) and a 2D ^{15}N TROSY-HSQC spectrum was recorded after the addition of each aliquot. Titrations were performed at 25 °C with spectra recorded on a 600 MHz Varian Unity-Inova spectrometer equipped with a *z*-gradient cold probe. The final molar ratio of HscB to IscU was 2. HscB-induced changes in amide peak positions of IscU, $\Delta\delta_{HN}$ (in parts per million), were calculated according to eq 1 (*32*)

$$\Delta\boldsymbol{\delta}_{HN} = [(\Delta\boldsymbol{\delta}_H)^2 + (\Delta\boldsymbol{\delta}_N/6)^2]^{1/2} \quad (1)$$

where $\Delta\delta_H$ and $\Delta\delta_N$ are the chemical shift changes in the proton and nitrogen dimensions, respectively.

Isothermal Titration Calorimetry. ITC measurements were taken at 25 °C in 50 mM HEPES (pH 7.5), 150 mM NaCl, and 4 mM TCEP using a VP-ITC isothermal titration calorimeter (MicroCal LLC). The injection syringe contained 3.84 mM apo-IscU or 3.95 mM apo-IscU(D39A), and the sample cell contained 0.27 mM HscB. All solutions were thoroughly degassed by being stirred under vacuum before use. Each titration was started with an initial injection of 3 μL, followed by 34 injections of 8 μL with a 240 s gap between consecutive injections. The ORIGIN software supplied with the instrument was used to integrate the peaks of the thermograms and to fit each isotherm by nonlinear regression analysis to yield binding constants (K_a), enthalpies of binding (ΔH), and stoichiometries (n). Entropies of binding (ΔS) were calculated from the K_a and ΔH values by standard thermodynamic relationships. Estimated errors in K_a, ΔH, and n were generated automatically by the software. Because the heat produced upon injection of buffer into buffer was small (< 0.2 kcal/mol), the data presented in the text were not corrected for this effect. The heat of dilution of IscU was approximated from the heats of the last few injections in each series, and the data presented in the text are corrected for this effect.

ATPase Assays. ATPase rates were determined at 23 °C in HKM buffer [50 mM HEPES (pH 7.3), 150 mM KCl, and 10 mM $MgCl_2$] containing 1 mM ATP by measuring the amount of phosphate released using the EnzCheck coupled enzyme phosphate assay kit as described previously (*14*).

Sequence Alignment. TBLASTN was used to search for amino acid sequences of homologues to *E. coli* IscU. In addition to IscU homologues, these initial searches also identified many NifU- and SufU-type proteins. To screen out the latter, sequences lacking the ^{99}LPPVK^{103} (or a highly similar) HscA recognition

motif of *E. coli* IscU were discarded. The final 131 sequences were divided into seven groups: 9 vertebrates, 20 fungi/metazoa, 11 other eukaryotes, 11 α-proteobacteria, 28 β-proteobacteria, 46 γ-proteobacteria, and 6 other prokaryotes. Sequences of each group were aligned separately with ClustalW2 (*33*) using default parameters, and the alignment result within each group was analyzed to identify identical residues, and positions that had "conserved substitutions" or "semiconserved substitutions" as classified by ClustalW2 (*33*). The global sequence conservation pattern among all 131 sequences was evaluated by comparing the results of each group alignment and identifying residues that were identical, >90% similar, or >80% similar among all groups.

RESULTS

Two Interconverting Conformational States of Apo-IscU. Initial evidence of two conformational states of apo-IscU that interchange slowly on the NMR time scale came from the observation of two ^{15}N HSQC cross-peaks corresponding to the side chain of the single tryptophan residue in the protein (δ^1H 10.3 ppm and δ^{15}N 129.1 ppm, δ^1H 10.1 ppm and δ^{15}N 129.3 ppm; boxed signals of Figure 1A). In addition, the ^{15}N HSQC spectrum of apo-IscU exhibited two sets of signals; one had sharp and well-dispersed peaks, and the other had broad peaks that were overlapped in the center of the spectrum. While the former is characteristic of folded proteins, the latter is more typical of disordered proteins. The addition of $ZnCl_2$ caused the broad and overlapped signals in the center of the HSQC spectrum to disappear while most sharp and dispersed peaks were retained without significant peak shifts (Figure 1B). A similar observation was noted previously for *H. influenzae* IscU (*15*).

Unexpectedly, we found that the D39A substitution, which stabilizes the Fe−S cluster in holo-IscU (*5*−*8*), also stabilizes the more structured state of IscU. In the 2D ^{15}N HSQC spectrum of [U-^{15}N]apo-IscU(D39A), the peaks corresponding to the less structured state became very weak in intensity compared to those of the more structured conformation (Figure 1C). However, most cross-peaks exhibited only small shifts in position compared to apo-IscU. Thus, the D39A substitution shifts the equilibrium between the ordered and disordered states of IscU rather than altering its secondary or tertiary structure.

The extensive congruence between the spectra of Zn-IscU and apo-IscU(D39A) (Figure 1D) indicates that the zinc-bound state of IscU and the ordered state of apo-IscU stabilized by the D39A substitution have similar folds. The major differences between the two spectra correspond mainly to the peaks of apo-IscU(D39A) assigned (see below) to residues located in loop regions (C37, G38, V40−L43, G62, C63, S69−S71, V73, T74, K89, and N90) or in a portion of helix α5 (C106−L109, E111−A113, K115, and A117). These are residues involved in metal binding or that become ordered in Zn-IscU.

A 2D exchange spectrum (*27*, *28*) of apo-IscU (Figure 1E) revealed the presence of exchange cross-peaks linking the two Trp side chain peaks. This result confirmed that these two peaks originate from two exchanging conformations, rather than two covalently distinct protein species, and indicated that the two states have lifetimes in the millisecond to second range. The 2D exchange spectrum enabled us to identify other, linked pairs of signals in the 2D ^{15}N HSQC spectrum of [U-^{15}N]apo-IscU (Table S1 of the Supporting Information) that could be used to assign the backbone amide signals of residues D24−G28, G51−E54, L82−K89, and D92−L97 in both states (see below). We used the $^{13}C^{\alpha}$ and $^{13}C^{\beta}$ chemical shifts of these residues to analyze the secondary structure of the two conformational states (Figure 2). It has been shown that the difference between the secondary chemical shifts of $^{13}C^{\alpha}$ and $^{13}C^{\beta}$ ($\Delta\delta^{13}C^{\alpha} - \Delta\delta^{13}C^{\beta}$) is a reliable indicator of secondary structural elements (*30*, *31*). Our results indicate that residues E25, V27, I52, I53, L82−Q86, I88, K89, and D92−E96 form ordered secondary structural elements in the folded conformation, whereas these structural elements are only partially populated in the disordered conformation.

Resonance Assignments of Apo-IscU(D39A). Because of the diminished intensity of the broad and overlapped set of peaks, the NMR spectra of apo-IscU(D39A) were much easier to interpret than those of apo-IscU. Therefore, we concentrated first on assigning spectra of apo-IscU(D39A). Resonance assignments were achieved by employing samples of apo-IscU(D39A) that were uniformly labeled with ^{13}C and ^{15}N and selectively reverse-labeled. These efforts led to resonance assignments for residues K6−D9, R15−N22, D24−A34, C37−K59, G62, C63, S69−L99, V102−I104, and C106−K128. Notably, most of the unassigned residues were located in the N-terminal region or in loop regions observed to be involved in metal coordination in the zinc complex (*15*). We used the PECAN web server (*29*) to predict the secondary structural elements of apo-IscU(D39A) from its assigned chemical shifts and amino acid sequence. The results matched closely the secondary structure elements determined from the solution structure of *H. influenzae* Zn-IscU (*15*), except for the absence of the N-terminal helix α1 of Zn-IscU. We have used the designators for the corresponding secondary structural elements in *H. influenzae* Zn-IscU (*15*) in describing those in *E. coli* apo-IscU(D39A): strand β1, G28−G33; strand β2, V40−V47; strand β3, E54−K59; helix α2, S69−W76; helix α3, L82−Q86; helix α4, N90−L97; and helix α5, I104−K124.

Backbone Dynamics of Apo-IscU(D39A). We measured ^{15}N R_1 and R_2 relaxation rates and ^{1}H−^{15}N heteronuclear NOEs to investigate the backbone dynamics of apo-IscU(D39A) (Figure 3). The mean values of R_1, R_2, and the heteronuclear NOE were 1.64 ± 0.26 s^{-1}, 15.37 ± 3.90 s^{-1}, and 0.73 ± 0.29, respectively. The N- and C-terminal residues, and some residues in loop regions, including K6−D9, D21, N22, C37, G38, and A39, exhibited distinctively higher R_1 and lower ^{1}H−^{15}N NOE values characteristic of picosecond to nanosecond dynamics; the dynamic properties of these residues could account for the failure to detect signals from other residues in these regions (M1−E5, H10−N13, N23, and A36). Both the R_1 and R_2 values for residues F58, K59, G62, C63, and S69−S71 were slightly higher than average, which implies that the loop between strand β3 and helix α2 undergoes simultaneous picosecond to nanosecond and microsecond to millisecond dynamics. It is likely that the dynamic properties of this region are responsible for the failure to observe signals from residues T60, Y61, and G64−A68. Residues L97−L99, I108, and L109 had distinctively high R_2 values without either an increase in R_1 values or a decrease in ^{1}H−^{15}N NOE, suggesting that they are affected by a slow (microsecond to millisecond) chemical exchange process. It is of interest that this dynamic region includes the conserved ^{99}LPPVK^{103} motif known to interact with HscA (*20*, *21*).

Perturbations in the Chemical Shifts of Apo-IscU(D39A) upon Addition of HscB. To probe the effect of HscB on IscU, we collected a series of 2D ^{15}N TROSY-HSQC spectra of samples containing different molar ratios of [U-^{15}N]apo-IscU (D39A) and HscB. Peaks corresponding to residues K6−D9, R15, D21, N22, D24, N26−S29, A39, K46−D49, G51−D55,

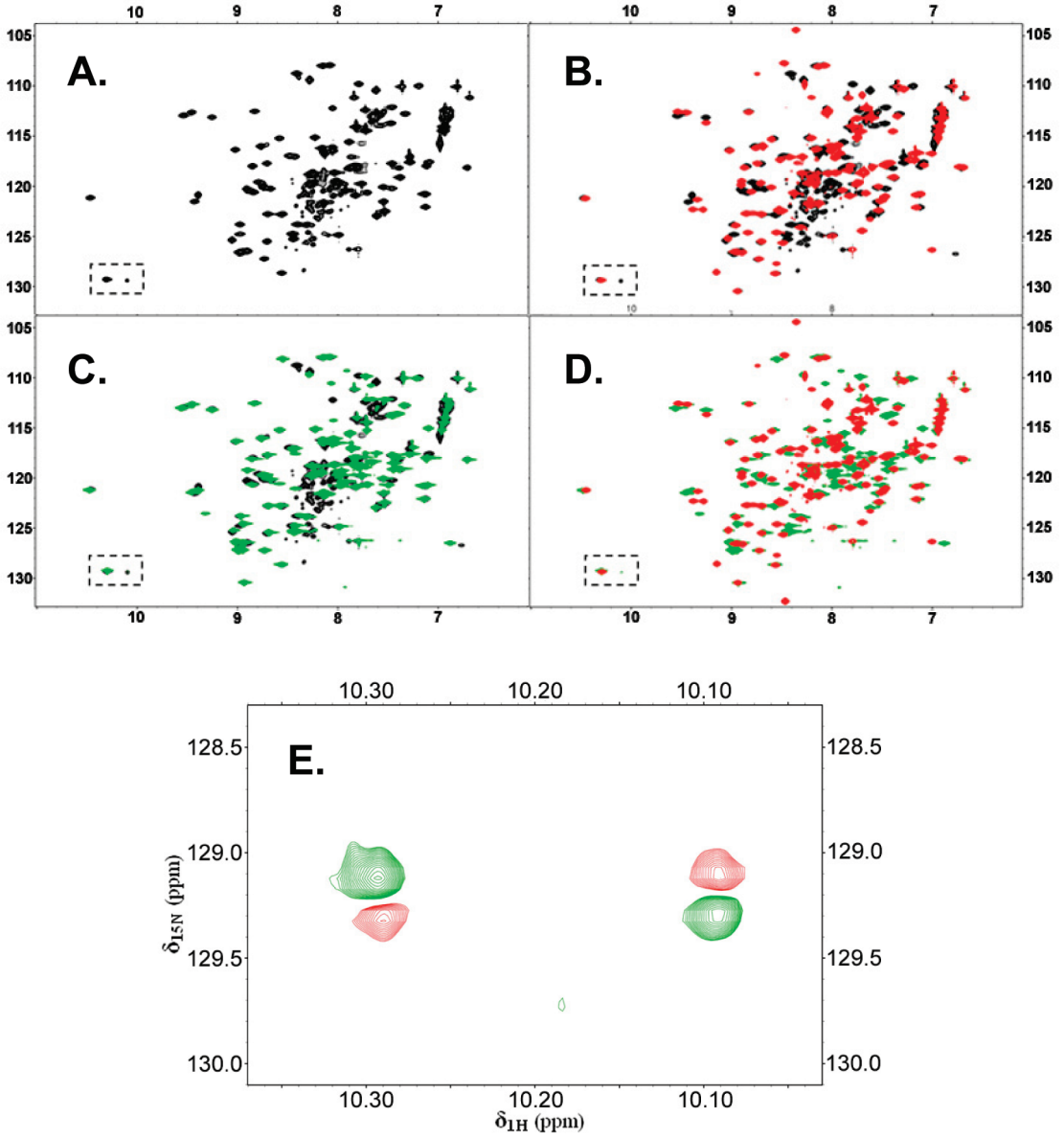

FIGURE 1: Evidence from 2D ^{15}N HSQC NMR spectra that *E. coli* apo-IscU exists in solution as two slowly interconverting conformational states and that the equilibrium is shifted either by zinc ion binding or by the single-site mutation D39A. The boxed region in panels A−D contains resonances from the single tryptophan residue, Trp76. (A) Spectrum of *E. coli* apo-IscU. Because IscU contains only a single Trp, the presence of cross-peaks in the boxed spectral region indicates the existence of two different conformations. (B) Spectrum of *E. coli* IscU in the presence of 3 mM $ZnCl_2$ (red) overlaid with the spectrum of apo-IscU (black). Zinc binding to IscU results in the disappearance of the minor Trp side chain peak as well as the cluster of broad peaks present in the central region of the spectrum of apo-IscU. (C) Spectrum of *E. coli* apo-IscU(D39A) (green) overlaid with the spectrum of apo-IscU (black). As with zinc binding, the D39A mutation leads to the disappearance of the minor Trp side chain signal and the cluster of broad and overlapped peaks in the central region of the spectrum of apo-IscU. (D) Spectrum of *E. coli* IscU in the presence of 3 mM $ZnCl_2$ (red) overlaid with the spectrum of *E. coli* apo-IscU(D39A) (green). The close correspondence between two spectra indicates that Zn-IscU and apo-IscU(D39A) are structurally similar. (E) Two-dimensional ^{1}H−^{15}N exchange spectrum (750 MHz Bruker DMX NMR spectrometer) of apo-IscU. Cross-peaks assigned to Trp76 (green) are connected by exchange cross-peaks (red). This result demonstrates that these two peaks originate not from two covalently distinct protein species but from two interchanging conformations.

R57, F58, S69, L72, V73, E75−A85, D92, E95, L97−L99, L109, and D120−K128 showed only minor chemical shift perturbations [< 0.04 ppm (Figure 4A)], suggesting that HscB has a minimal effect on these residues. Peaks corresponding to N16−F20, G38, M41, I45, A56, S70, S71, T74, Q86, T91, I93, A94, E96, V102−I104, S107, I108, A116, and A119 exhibited larger chemical shift perturbations [> 0.04 ppm (Figure 4A)], indicative of a more pronounced environmental change in the presence of HscB. A fraction of peaks, corresponding to residues E25, G30−A34, C37, V40, K42−Q44, K59, G62, C63, I88−N90, C106, E111−A113, K115, A117, and I118, exhibited only minor chemical shift perturbations before broadening beyond detection at substoichiometric amounts of HscB (Figure 4A). These peaks disappeared from the HSQC spectrum at an HscB:IscU ratio of ~0.4.

To exclude the possibility that the observed chemical shift perturbations are caused by a nonspecific protein−protein interaction, we collected 2D ^{15}N TROSY-HSQC spectra of [U-^{15}N] apo-IscU(D39A) mixed with various amounts of HscB(L92A/M93A/F153A). This HscB mutant was shown previously to be defective in achieving maximal stimulation of HscA ATPase activity in the presence of IscU and also increased the concentration of IscU required for half-maximal stimulation from ≅3 to 24 μM (*22*). Indeed, not only did we observe no line

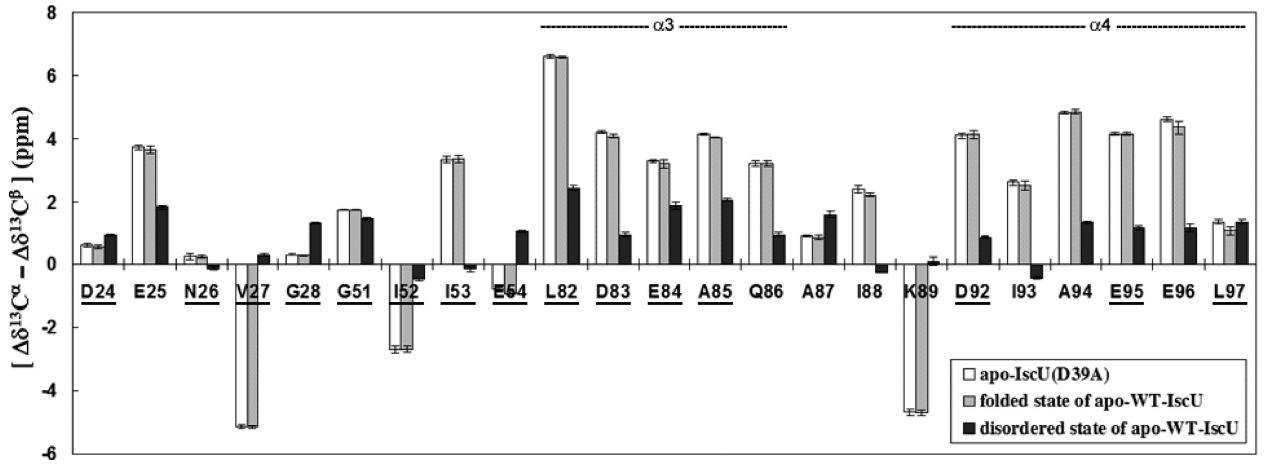

FIGURE 2: Comparison of the predictor of secondary structure ($\Delta\delta^{13}C^{\alpha} - \Delta\delta^{13}C^{\beta}$) (*30*, *31*) for corresponding residues in (white bars) apo-IscU (D39A), (gray bars) the ordered state of apo-IscU, and (black bars) the disordered state of apo-IscU. Positive values of $\Delta\delta^{13}C^{\alpha} - \Delta\delta^{13}C^{\beta}$ indicate α-helix and negative values β-strand. Values near zero indicate random coil. Note the close agreement between the $\Delta\delta^{13}C^{\alpha} - \Delta\delta^{13}C^{\beta}$ values for residues in the ordered state of apo-IscU and those for apo-IscU(D39A). Comparison of the $\Delta\delta^{13}C^{\alpha} - \Delta\delta^{13}C^{\beta}$ values for the ordered and disordered forms of IscU indicates that helix α3 in the disordered state is populated at ~33−50% and that helix α4 in the disordered state is populated at ~25−33%. The results suggest that the two conformational states of apo-IscU interconvert by means of an order−disorder transition affecting the stability of helices α3 and α4. Residues of apo-IscU(D39A) that show minimal chemical shift changes upon formation of the HscB complex are underlined. This result shows that the ordered state of apo-IscU is stabilized upon complex formation and that the underlined residues probably do not contact HscB. Only residues Q86 (part of helix α3) and I93, A94, and E95 (part of helix α4) exhibit shifts upon complex formation.

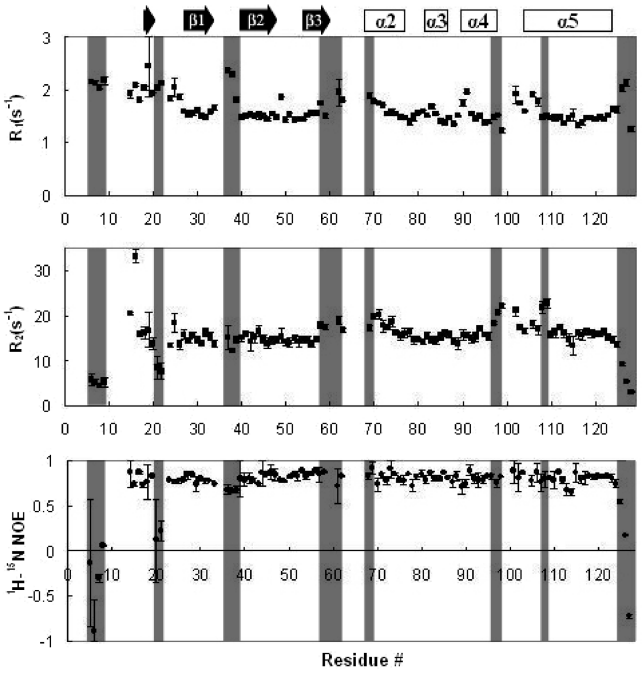

FIGURE 3: R_1 and R_2 relaxation rates and $^1H-^{15}N$ heteronuclear NOE results for *E. coli* apo-IscU(D39A) plotted as a function of peptide sequence. Data were collected at 600 MHz (^1H) and 25 °C. Blank regions correspond to residues whose signals were either not observed or not assigned. Error bars indicate the standard deviation from two replicate data sets acquired under the same conditions. Some of the residues showing distinctive relaxation rates or NOE values are shaded for the sake of comparison. Secondary structural elements predicted from the assigned chemical shifts are indicated at the top.

broadening effect in the spectrum of [U-^{15}N]apo-IscU(D39A) mixed with 3 equiv of HscB(L92A/M93A/F153A), but chemical shift changes were also negligible (data not shown). On the basis of these results, we conclude that the observed chemical shift perturbation and line broadening effects noted earlier arise from a specific interaction between apo-IscU(D39A) and HscB.

Resonance Assignments of Apo-IscU Complexed with HscB. To ascertain whether apo-IscU(D39A) and apo-IscU behave similarly when interacting with HscB, we also conducted a titration experiment using [U-^{15}N]apo-IscU and HscB. Although we were unable to achieve complete resonance assignments for apo-IscU, because of severe spectral overlaps and ambiguities arising from the presence of two distinct conformations, we could assign some signals by comparing their positions with peaks from apo-IscU(D39A). We were then able to partially extend these assignments with additional NMR experiments. The chemical shift perturbation pattern observed for the assignable resonances of apo-IscU in the presence of 2.2 equiv of HscB was similar to that obtained for apo-IscU(D39A) (Figure 4B). Backbone amide signals from residues N16, G18, F20, D24, E25, S29, I45, E54, R57, V73, T74, W76, V77, A85−A87, N90, E96, L97, V102−I104, I108, I114, and A116 exhibited shifts of >0.036 ppm, while those from G30−A34, L43, Q44, K59, C106, S107, A110, E111, and A113 suffered extreme line broadening.

DISCUSSION

The Isc system is an important and complex multiprotein system. Its importance is linked to its highly conserved, "housekeeping" Fe−S cluster assembly and transfer activity, while its complexity derives from the involvement of several proteins (CyaY, IscR, IscS, IscU, IscA, HscB, HscA, and ferredoxins) and the challenges of determining the mechanisms for Fe−S cluster assembly and transfer (*2*). In these mechanisms, an understanding of the versatile and dynamic functions of IscU has remained particularly elusive. Previous studies suggested that IscU, as a scaffold protein in the "generalized" Fe−S cluster biosynthesis system, needs to have considerable flexibility to be capable of transferring Fe−S clusters efficiently to a wide range of apoproteins (*17*, *18*); on the other hand, IscU needs to have a stable structural fold to maintain meaningful interactions with

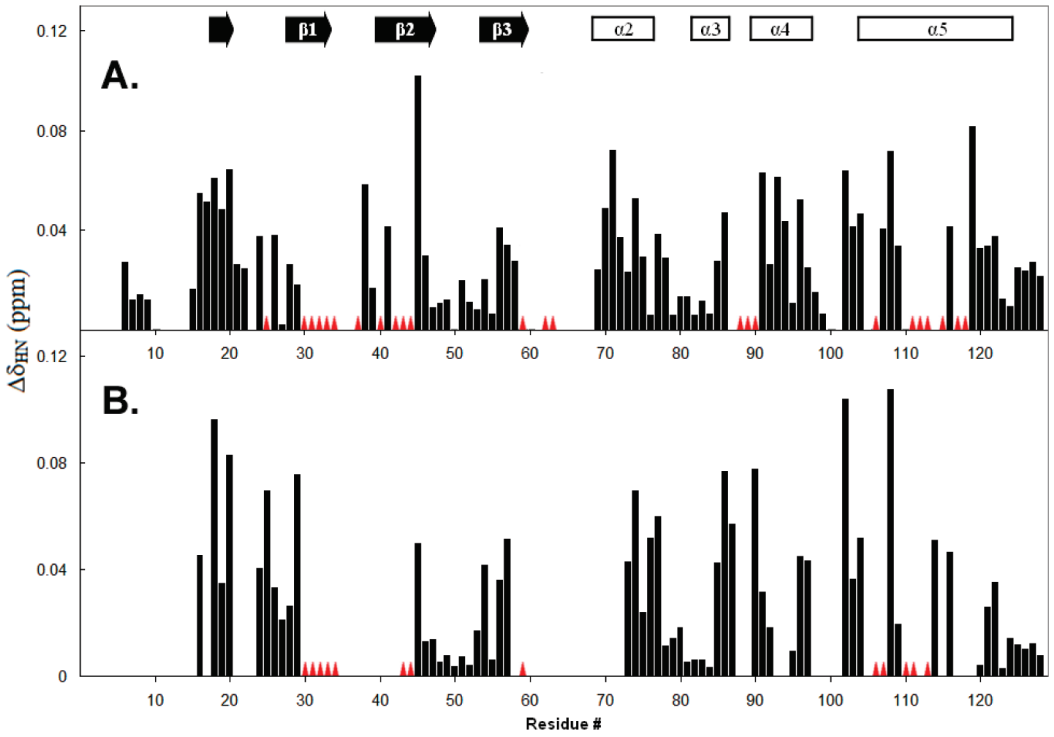

FIGURE 4: Chemical shift perturbations ($\Delta\delta_{HN}$) plotted as a function of the IscU peptide sequence of (A) apo-IscU(D39A) upon the addition of 2 equiv of HscB and (B) apo-IscU upon the addition of 2.2 equiv of HscB. Blank regions correspond to residues whose signals were not observed or not assigned. Red triangles denote residues for which chemical shift perturbation could not be determined, because the signals broadened out completely or shifted discontinuously to unknown locations. Secondary structural elements predicted from the assigned chemical shifts are indicated at the top.

various protein components of the Isc system (e.g., IscS, HscB, and HscA). The solution structures of the nonphysiological, Zn-bound forms of IscU from *H. influenzae* (*15*) and *M. musculus* (PDB entry 1wfz) gave static pictures of the protein structure and did not explain the reported versatility of IscU. Rather, the recent crystal structure of holo-IscU from *A. aeolicus* (*16*) and the solution structural study of *T. maritima* apo-SufU (*17*, *18*), a homologue of IscU, provided consistent evidence of structural flexibility.

This study of *E. coli* apo-IscU provides more direct evidence of the dynamic nature of IscU. Our NMR results indicate that IscU in solution populates two major conformations that interchange slowly. One conformation is largely disordered, and the other is largely structured except for the metal-binding regions, which remain dynamically disordered such that their NMR signals were not observed. From this observation arises an intriguing hypothesis that two different conformations of IscU may serve different functions. It would be reasonable to speculate that the ordered conformation is appropriate to scaffold the Fe−S cluster and that the disordered conformation serves to facilitate cluster transfer.

We also found that both the binding of zinc ion and the D39A mutation shift the equilibrium toward the structured conformation. IscU(D39A) has been found to reconstitute a more stable holo complex than IscU (*5*−*8*), but with a decreased rate of cluster transfer to apoferredoxin (*7*, *9*). It was suggested that the stabilization of the Fe−S cluster assembled on IscU(D39A) was a consequence of its being less solvent-accessible than that on holo-IscU (*9*, *10*). Our results suggest that the increased stability may result from the fact that the D39A mutation energetically stabilizes the structured state of IscU that is required for the holo complex. As discussed above, it is tempting to speculate that the slow step of the cluster transfer reaction is the opening of IscU to allow release of the cluster, and that this opening is accelerated by an order−disorder transition in IscU. Because the order−disorder transition is diminished in IscU(D39A), this could explain the lower transfer rate observed with this mutant (*7*, *9*).

Signals showing exchange cross-peaks in the exchange spectrum of apo-IscU are localized primarily to helices α3 and α4. Our results indicate that helices α3 and α4 undergo conformational exchange between an ordered secondary structure and a random coil-like conformation (Figure 2). By contrast, the neighboring region, including helix α2 and the adjacent loop containing the ^{99}LPPVK^{103} motif, are only slightly affected by the presence of HscB, suggesting that this region, which is known to bind HscA (*20*, *21*), remains flexible and accessible after formation of the IscU·HscB complex. The crystal structure of the complex between HscA and ELPPVKIHC suggested, however, that IscU must undergo a conformational change to form the complex (*19*). This result raises the possibility that the order−disorder transition of helices α3 and α4 of IscU, which are adjacent to the binding motif, is somehow coupled to the binding interaction with HscA.

Our NMR results indicate that the residues of apo-IscU (D39A) most perturbed in the presence of HscB are localized primarily in the first two β-strands (β1 and β2) and the last α-helix (α5) of the scaffold protein (Figure 5A). The same pattern of perturbed residues is seen also for the structured form of apo-IscU (Figure 5B), although fewer assignments are available. A comprehensive sequence analysis of IscU homologues shows that these regions are highly conserved from proteobacteria to vertebrates (Figure 6).

Our chemical shift perturbation results indicated that several hydrophobic residues in the first two β-strands of apo-IscU(D39A),

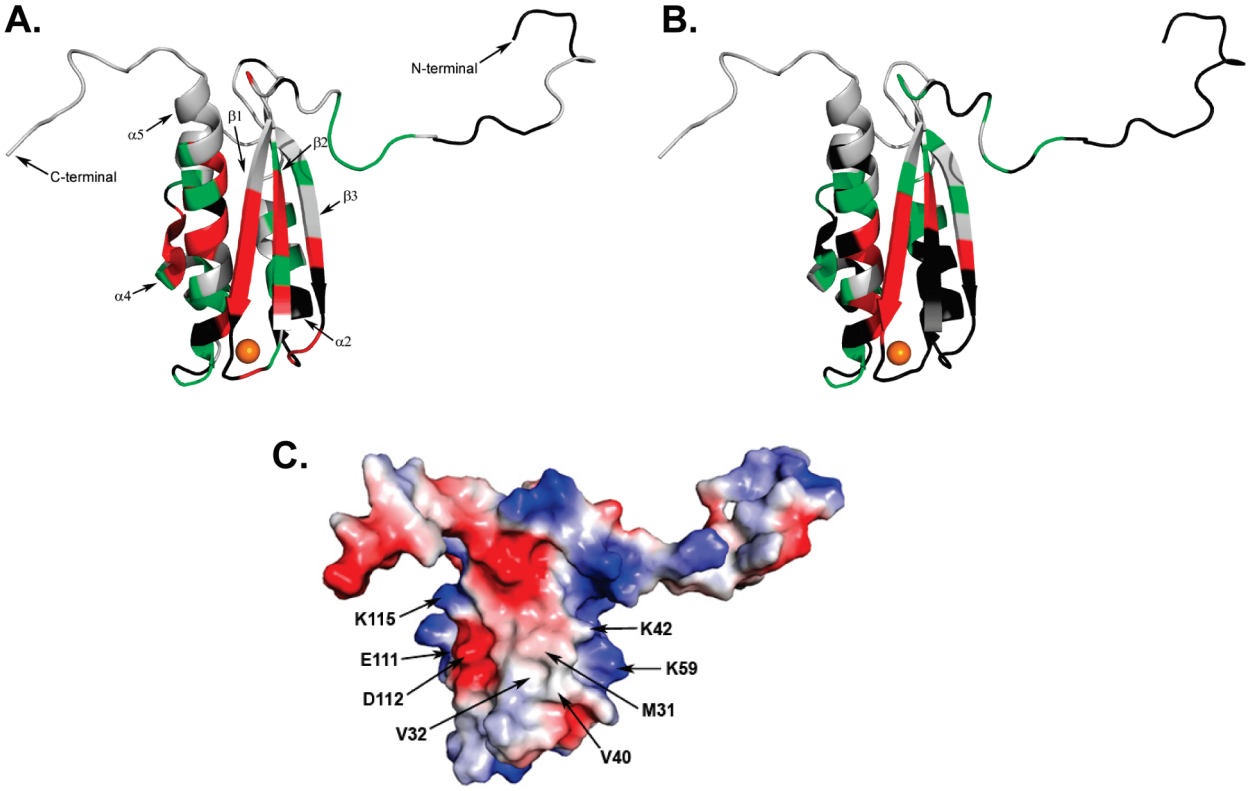

FIGURE 5: Putative surface of apo-IscU that interacts with HscB. (A) Chemical shift perturbations of apo-IscU(D39A) resulting from the addition of HscB mapped onto the structure of *H. influenzae* Zn-IscU (PDB entry 1r9p) (*15*). Red indicates residues whose signals broadened beyond detection; green indicates residues with large ($\Delta\delta_{HN} > 0.04$ ppm) chemical shift changes, and black indicates residues whose signals could not be assigned or followed during the titration. The zinc atom is colored orange. (B) Chemical shift perturbations of apo-IscU resulting from the addition of HscB mapped onto the structure of *H. influenzae* Zn-IscU (*15*). Red indicates residues whose signals broadened beyond detection; green indicates residues with large ($\Delta\delta_{HN} > 0.036$ ppm) chemical shift changes, and black indicates residues whose signals could not be assigned or followed during the titration. (C) Surface electrostatic potential of *H. influenzae* Zn-bound IscU. Neutral potential is shaded white, negative surface potential red, and positive surface potential blue. Residues proposed to be involved in the binding interaction with HscB are labeled.

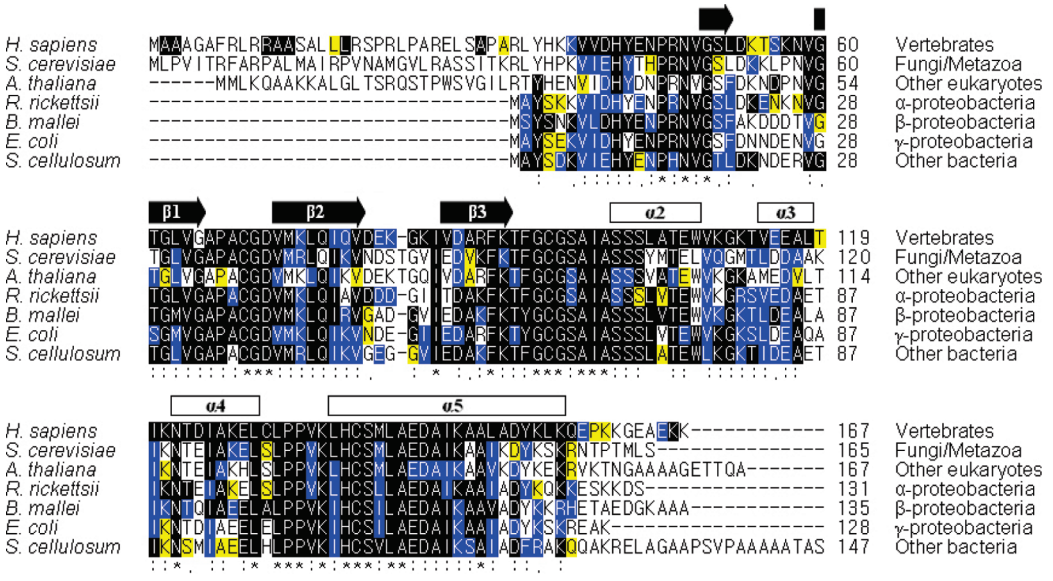

FIGURE 6: Sequence alignment of IscU homologues. A total of 131 aligned sequences were divided into seven groups: 9 sequences of vertebrates, 20 of fungi/metazoa, 11 of other eukaryotes, 11 of α-proteobacteria, 28 of *β*-proteobacteria, 46 of *γ*-proteobacteria, and 6 of other prokaryotes. For the sake of simplicity, the figure shows representative aligned sequences from each of the seven groups. Sequence conservation within each group is represented by three colors: black for total conservation within the group, blue for only conserved substitutions within the group, and yellow for only semiconserved substitutions within the group. The level of global conservation in the 131 sequences is represented by three symbols: asterisk for residues identically conserved in all sequences, colon for >90% similarity in all sequences, and period for >80% similarity in all sequences. The secondary structural elements predicted from this study of *E. coli* IscU(D39A) are indicated at the top.

namely M31, V32, V40, and L43, were highly perturbed upon addition of HscB (Figure 4A). Because the hydrophobic side chains of M31 and V40 are solvent exposed in the solution structure of *H. influenzae* Zn-IscU (Figure 5C), we speculate that these two

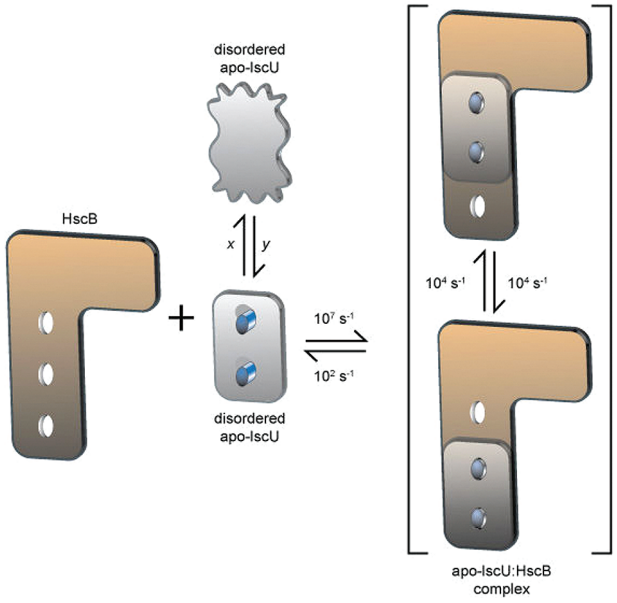

FIGURE 7: Cartoon depicting the dynamic interactions between apo-IscU and HscB that explain the extreme broadening of signals from IscU (HscB) upon the addition of substoichiometric amounts of HscB (IscU). Apo-IscU exists as an equilibrium between a disordered and ordered state. The rates x and y are similar in magnitude, because the two states have nearly equal populations. Individually, x and y must be slower than 10 s^{-1} to explain the observation of separate signals for the disordered and ordered state, but faster than 0.3 s^{-1} to account for the observation of 2D exchange peaks. The ordered state of apo-IscU binds to HscB, but the complex formed undergoes a dynamic rearrangement that is faster than the off rate for dissociation of the complex. The change occurring within the complex could involve the relative displacement of the two proteins, as depicted here, or a rearrangement of hydrophobic groups in the contact area without a relative displacement. The NMR signals of IscU and HscB that become excessively broadened upon complex formation must have appreciable chemical shift differences in the two bound states. The rates shown are crude estimates (see the text).

residues are involved in a hydrophobic interaction in the IscU−HscB complex. The NMR signals of a number of highly conserved charged residues of apo-IscU were also perturbed in the presence of HscB. These include K42 and K59 in strands β2 and β3, which are located at the boundary of the hydrophobic patch with their charged side chains exposed to solvent (Figure 5C), as well as residues E111, D112, and K115 in helix α5 (Figure 5C). Whereas M31 and V40 might provide stability to the complex, the charged residues may be important for conferring specificity and/or strengthening the interaction. Consistent with these results, the proposed binding site of IscU on HscB includes a highly conserved, solvent-exposed hydrophobic patch as well as an acidic triad of glutamates (*22*).

The results (Figure 4) indicate that binding to HscB stabilizes the ordered state of apo-IscU. Signals from most of the residues that exhibited large chemical shift differences between the ordered and disordered forms of apo-IscU remained at their ordered positions [equivalent to those of apo-IscU(D39A) upon addition of HscB (Figure 2)].

A challenging aspect of the apo-IscU−HscB interaction is the excessive line broadening that affects a large number of HSQC cross-peaks (Figure 4). Broadening occurs at substoichiometric concentrations of added HscB, and the peaks do not sharpen upon saturation of apo-IscU with bound HscB. For these reasons, the effect cannot be explained by simple association−dissociation kinetics. Explanation of the effect requires a dynamic structural rearrangement of the bound complex at a rate much faster that the dissociation rate for the complex. At substoichiometric concentrations of added HscB, signals from nuclei with appreciably different chemical shifts in the distinct bound states are saturated as a result of the interconversion, and this saturation is transferred to the pool of uncomplexed IscU. The rearrangement may involve shuffling of hydrophobic residues in the contact region between the two proteins or shifting of the complex between two (or more) orientations.

The schematic diagram presented in Figure 7 illustrates our finding that HscB binds to the ordered state of apo-IscU and depicts the simplest kind of rearrangement that would explain the substoichiometric broadening of NMR signals from apo-IscU reported here as well as those from HscB as reported previously (*22*). The rates shown are approximations based on the known dissociation constant (≅10 μM), an assumed association rate of 10^7 s^{-1}, and assumed chemical shift differences of ∼0.5 ppm (300 and 400 s^{-1} for ^{1}H at 600 and 800 MHz, respectively) for the affected peaks in the interconverting states. This model can be tested and the rates refined by future NMR experiments that we are planning to undertake.

ACKNOWLEDGMENT

We thank Robin Davies for drafting Figure 7.

SUPPORTING INFORMATION AVAILABLE

Chemical shifts of exchange cross-peaks observed in the 2D exchange spectrum of [U-^{15}N]apo-IscU (Table S1), evidence that IscU(D39A) forms a 1:1 complex with HscB with a binding affinity of ∼10 μM and thermodynamic parameters similar to those observed with wild-type IscU (Figure S1), and assay results showing that apo-IscU(D39A) acts synergistically with HscB to stimulate HscA ATPase activity in a manner similar to that observed for wild-type IscU (Figure S2). This material is available free of charge via the Internet at http://pubs.acs.org.

REFERENCES

(1) Beinert, H., Holm, R. H., and Munck, E. (1997) Iron-sulfur clusters: Nature's modular, multipurpose structures. *Science 277*, 653–659.
(2) Johnson, D. C., Dean, D. R., Smith, A. D., and Johnson, M. K. (2005) Structure, function, and formation of biological iron-sulfur clusters. *Annu. Rev. Biochem. 74*, 247–281.
(3) Zheng, L., Cash, V. L., Flint, D. H., and Dean, D. R. (1998) Assembly of iron-sulfur clusters. Identification of an iscSUA-hscBA-fdx gene cluster from *Azotobacter vinelandii*. *J. Biol. Chem. 273*, 13264–13272.
(4) Bonomi, F., Iametti, S., Ta, D. T., and Vickery, L. E. (2005) Multiple turnover transfer of [2Fe2S] clusters by the iron-sulfur cluster assembly scaffold proteins IscU and IscA. *J. Biol. Chem. 280*, 29513–29518.
(5) Unciuleac, M. C., Chandramouli, K., Naik, S., Mayer, S., Huynh, B. H., Johnson, M. K., and Dean, D. R. (2007) In vitro activation of apo-aconitase using a [4Fe-4S] cluster-loaded form of the IscU [Fe-S] cluster scaffolding protein. *Biochemistry 46*, 6812–6821.
(6) Shimomura, Y., Kamikubo, H., Nishi, Y., Masako, T., Kataoka, M., Kobayashi, Y., Fukuyama, K., and Takahashi, Y. (2007) Characterization and crystallization of an IscU-type scaffold protein with bound [2Fe-2S] cluster from the hyperthermophile, *Aquifex aeolicus*. *J. Biochem. 142*, 577–586.
(7) Wu, G., Mansy, S. S., Wu, S. P., Surerus, K. K., Foster, M. W., and Cowan, J. A. (2002) Characterization of an iron-sulfur cluster assembly protein (ISU1) from *Schizosaccharomyces pombe*. *Biochemistry 41*, 5024–5032.
(8) Foster, M. W., Mansy, S. S., Hwang, J., Penner-Hahn, J. E., Surerus, K. K., and Cowan, J. A. (2000) A mutant human IscU protein contains a stable [2Fe-2S]$^{2+}$ center of possible functional significance. *J. Am. Chem. Soc. 122*, 6805–6806.

(9) Wu, S. P., Wu, G., Surerus, K. K., and Cowan, J. A. (2002) Iron-sulfur cluster biosynthesis. Kinetic analysis of [2Fe-2S] cluster transfer from holo ISU to apo Fd: Role of redox chemistry and a conserved aspartate. *Biochemistry 41*, 8876–8885.
(10) Mansy, S. S., and Cowan, J. A. (2004) Iron-sulfur cluster biosynthesis: Toward an understanding of cellular machinery and molecular mechanism. *Acc. Chem. Res. 37*, 719–725.
(11) Chandramouli, K., and Johnson, M. K. (2006) HscA and HscB stimulate [2Fe-2S] cluster transfer from IscU to apoferredoxin in an ATP-dependent reaction. *Biochemistry 45*, 11087–11095.
(12) Bonomi, F., Iametti, S., Morleo, A., Ta, D., and Vickery, L. E. (2008) Studies on the mechanism of catalysis of iron-sulfur cluster transfer from IscU[2Fe2S] by HscA/HscB chaperones. *Biochemistry 47*, 12795–12801.
(13) Silberg, J. J., Hoff, K. G., Tapley, T. L., and Vickery, L. E. (2001) The Fe/S assembly protein IscU behaves as a substrate for the molecular chaperone Hsc66 from *Escherichia coli*. *J. Biol. Chem. 276*, 1696–1700.
(14) Hoff, K. G., Silberg, J. J., and Vickery, L. E. (2000) Interaction of the iron-sulfur cluster assembly protein IscU with the Hsc66/Hsc20 molecular chaperone system of *Escherichia coli*. *Proc. Natl. Acad. Sci. U.S.A. 97*, 7790–7795.
(15) Ramelot, T. A., Cort, J. R., Goldsmith-Fischman, S., Kornhaber, G. J., Xiao, R., Shastry, R., Acton, T. B., Honig, B., Montelione, G. T., and Kennedy, M. A. (2004) Solution NMR structure of the iron-sulfur cluster assembly protein U (IscU) with zinc bound at the active site. *J. Mol. Biol. 344*, 567–583.
(16) Shimomura, Y., Wada, K., Fukuyama, K., and Takahashi, Y. (2008) The asymmetric trimeric architecture of [2Fe-2S] IscU: Implications for its scaffolding during iron-sulfur cluster biosynthesis. *J. Mol. Biol. 383*, 133–143.
(17) Bertini, I., Cowan, J. A., Del Bianco, C., Luchinat, C., and Mansy, S. S. (2003) *Thermotoga maritima* IscU. Structural characterization and dynamics of a new class of metallochaperone. *J. Mol. Biol. 331*, 907–924.
(18) Mansy, S. S., Wu, S. P., and Cowan, J. A. (2004) Iron-sulfur cluster biosynthesis. Biochemical characterization of the conformational dynamics of *Thermotoga maritima* IscU and the relevance for cellular cluster assembly. *J. Biol. Chem. 279*, 10469–10475.
(19) Cupp-Vickery, J. R., Peterson, J. C., Ta, D. T., and Vickery, L. E. (2004) Crystal structure of the molecular chaperone HscA substrate binding domain complexed with the IscU recognition peptide ELPPVKIHC. *J. Mol. Biol. 342*, 1265–1278.
(20) Hoff, K. G., Ta, D. T., Tapley, T. L., Silberg, J. J., and Vickery, L. E. (2002) Hsc66 substrate specificity is directed toward a discrete region of the iron-sulfur cluster template protein IscU. *J. Biol. Chem. 277*, 27353–27359.
(21) Hoff, K. G., Cupp-Vickery, J. R., and Vickery, L. E. (2003) Contribution of the LPPVK motif of the iron-sulfur template protein IscU to interactions with the Hsc66-Hsc20 chaperone system. *J. Biol. Chem. 278*, 37582–37589.
(22) Füzéry, A. K., Tonelli, M., Ta, D. T., Cornilescu, G., Vickery, L. E., and Markley, J. L. (2008) Solution structure of the iron-sulfur cluster cochaperone HscB and its binding surface for the iron-sulfur assembly scaffold protein IscU. *Biochemistry 47*, 9394–9404.
(23) Jones-Mortimer, M. C. (1968) Positive control of sulphate reduction in *Escherichia coli*. Isolation, characterization and mapping of cysteineless mutants of *E. coli* K12. *Biochem. J. 110*, 589–595.
(24) Muchmore, D. C., McIntosh, L. P., Russell, C. B., Anderson, D. E., and Dahlquist, F. W. (1989) Expression and nitrogen-15 labeling of proteins for proton and nitrogen-15 nuclear magnetic resonance. *Methods Enzymol. 177*, 44–73.
(25) Delaglio, F., Grzesiek, S., Vuister, G. W., Zhu, G., Pfeifer, J., and Bax, A. (1995) NMRPipe: A multidimensional spectral processing system based on UNIX pipes. *J. Biomol. NMR 6*, 277–293.
(26) Goddard, T. D., and Kneller, D. G. (2008) SPARKY 3 , University of California, San Francisco.
(27) Wider, G., Neri, D., and Wuthrich, K. (1991) Studies of slow conformational equilibria in macromolecules by exchange of heteronuclear longitudinal 2-spin-order in a 2D difference correlation experiment. *J. Biomol. NMR 1*, 93–98.
(28) Mori, S., Abeygunawardana, C., Johnson, M. O., and van Zijl, P. C. (1995) Improved sensitivity of HSQC spectra of exchanging protons at short interscan delays using a new fast HSQC (FHSQC) detection scheme that avoids water saturation. *J. Magn. Reson., Ser. B 108*, 94–98.
(29) Eghbalnia, H. R., Wang, L., Bahrami, A., Assadi, A., and Markley, J. L. (2005) Protein energetic conformational analysis from NMR chemical shifts (PECAN) and its use in determining secondary structural elements. *J. Biomol. NMR 32*, 71–81.
(30) Wang, L., Eghbalnia, H. R., Bahrami, A., and Markley, J. L. (2005) Linear analysis of carbon-13 chemical shift differences and its application to the detection and correction of errors in referencing and spin system identifications. *J. Biomol. NMR 32*, 13–22.
(31) Wang, L., Eghbalnia, H. R., and Markley, J. L. (2006) Probabilistic approach to determining unbiased random-coil carbon-13 chemical shift values from the protein chemical shift database. *J. Biomol. NMR 35*, 155–165.
(32) Farmer, B. T.II, Constantine, K. L., Goldfarb, V., Friedrichs, M. S., Wittekind, M., Yanchunas, J.Jr., Robertson, J. G., and Mueller, L. (1996) Localizing the $NADP^+$ binding site on the MurB enzyme by NMR. *Nat. Struct. Biol. 3*, 995–997.
(33) Chenna, R., Sugawara, H., Koike, T., Lopez, R., Gibson, T. J., Higgins, D. G., and Thompson, J. D. (2003) Multiple sequence alignment with the Clustal series of programs. *Nucleic Acids Res. 31*, 3497–3500.